https://doi.org/10.5194/gchron-2024-1
Preprint. Discussion started: 25 January 2024

The daughter-parent plot: a tool for analyzing thermochronological data

Birk Härtel and Eva Enkelmann

Department of Earth, Energy and Environment, University of Calgary, Calgary, T2L 1N4, Canada

Correspondence to: Birk Härtel (birk.haertel@ucalgary.ca)

Abstract. Plots of daughter against parent concentration (D-P plots) are widely used as isotope ratio plots in geochronology. Their main purposes are: (1) to visualize the main ingredient of the radiometric age equation – the daughter-parent ratio – and (2) to inspect the daughter-parent relationship for anomalous behavior indicating influences of geological processes or analytical bias. Despite their benefits, D-P plots are currently not used for analyzing low-temperature thermochronology data. This contribution aims at putting D-P plots on the map as a data analysis tool. We present a simple, decision-tree-based classification for daughter-parent relationships that places a dataset into one of seven classes: linear relationship with zero intercept, cluster, linear relationship with systematic offset, non-linear relationship, several age populations, scattered data, and inverse relationship. Assigning a class to a dataset enables to choose further data analysis steps and the right algorithm to calculate a sample age, e.g. as pooled, central or isochron age, or a range of ages. We discuss how to deal with small sample sizes and the possibility of comparing data across samples and chronometers. Our simple classification scheme uses the information in the D-P plot for facilitating thermochronological data analysis and making it more consistent and traceable.

1 Introduction

Plots of radiogenic daughter (D) vs. radioactive parent (P) concentrations (D-P plots, isochron plots) or their isotopic ratios are a standard tool for analyzing geochronological data (e.g., Kulp et al., 1952; Nicolaysen, 1961), such as U-Pb, Ar-Ar or Rb-Sr data. The main reason for their use is that the daughter-parent ratio is the main ingredient of determining a radiometric age. Furthermore, the D-P plot also enables us to visualize anomalous features in the data, such as outliers, excess daughters, parent loss, etc. Surprisingly, D-P plots have no wide application in low-temperature thermochronology, despite several authors suggesting them for the fission-track (FT) and (U-Th)/He (He) dating methods (Green, 1981; Wernicke and Lippolt, 1993; Dunkl, 2002; Vermeesch, 2008). The D-P plot allows a different perspective on thermochronological data than the commonly used age-(e)U, radial or age-grain size plots (Vermeesch, 2008; Flowers et al., 2022; Härtel et al., 2022a). It also helps to identify potentially problematic factors such as 'parentless helium' (Vermeesch, 2008) and provides criteria for selecting an appropriate age to report for a sample, e.g. as a mean, pooled, central, isochron age etc. (Vermeesch, 2008; Härtel et al., 2022a).

https://doi.org/10.5194/gchron-2024-1
Preprint. Discussion started: 25 January 2024

This article aims at proposing the D-P plot as a first step for analyzing FT, He or zircon Raman (ZR) data. We first discuss the background of the D-P plot and classify the commonly observed daughter-parent relationships. Then, we present a workflow for analyzing daughter-parent relationships. Based on each of these relationships, we suggest further steps of data analysis and calculation algorithms for sample ages. We then present a set of example data and finally discuss the use and limitation of D-P plots for small datasets, multiple samples, and detrital thermochronology. Our D-P-based approach to analyze thermochronological data is easily integrated into any FT, He, or ZR analysis and allows thermochronologists to trace their decisions during data analysis.

2 Background

2.1 Deriving the D-P plot

Using a plot of daughter (D) against parent (P) concentration rests upon the general age equation:

$$t = \frac{1}{\lambda} \ln\left(1 + c\,\frac{D}{P}\right) \qquad (1),$$

where t is the age, λ is the decay constant, and c is a constant to balance out the units of D and P. The actual quantities of D and P depend on the dating method. For FT dating, D are the spontaneous-track densities and P are either the induced track densities (i.e. external detector method) or U concentration measured using a LA-ICP-MS. For (U-Th)/He dating, the α-ejection corrected He concentration represent the daughter concentration. However, defining a parent concentration is difficult, because several α-emitting nuclides – ^{238}U, ^{235}U, ^{232}Th (and ^{147}Sm) – have to be considered. One solution is to express the parents as an effective uranium concentration (eU) – the sum of the parent concentrations weighted by their relative He production rate (e.g., Härtel et al., 2023), and thereby reduce the number of parents to one:

$$eU = 1.05\,[U] + 0.24\,[Th] + 0.0012\,[Sm] \qquad (2).$$

Appendix A discusses the formulation of eU in Eq. (2) and its differences to others (e.g., Shuster et al., 2006; Cooperdock et al., 2019). For ZR dating, the radiation-damage density represents the daughter concentration and the parent concentration is eU, similar to the He dating method. Appendix B provides additional discussion on the choice of daughter and parent concentration units for different dating methods.

2.2 Data patterns for multi-grain samples

It is evident from (1) that the age has a one-to-one relationship with the ratio D/P. Therefore, the position of a data point in a plot of D vs. P indicates the single-grain age by the slope of a tie line connecting it to the origin of the plot (Fig. 1). The D-P plot is thus the graphical representation of the age equation.

https://doi.org/10.5194/gchron-2024-1
Preprint. Discussion started: 25 January 2024

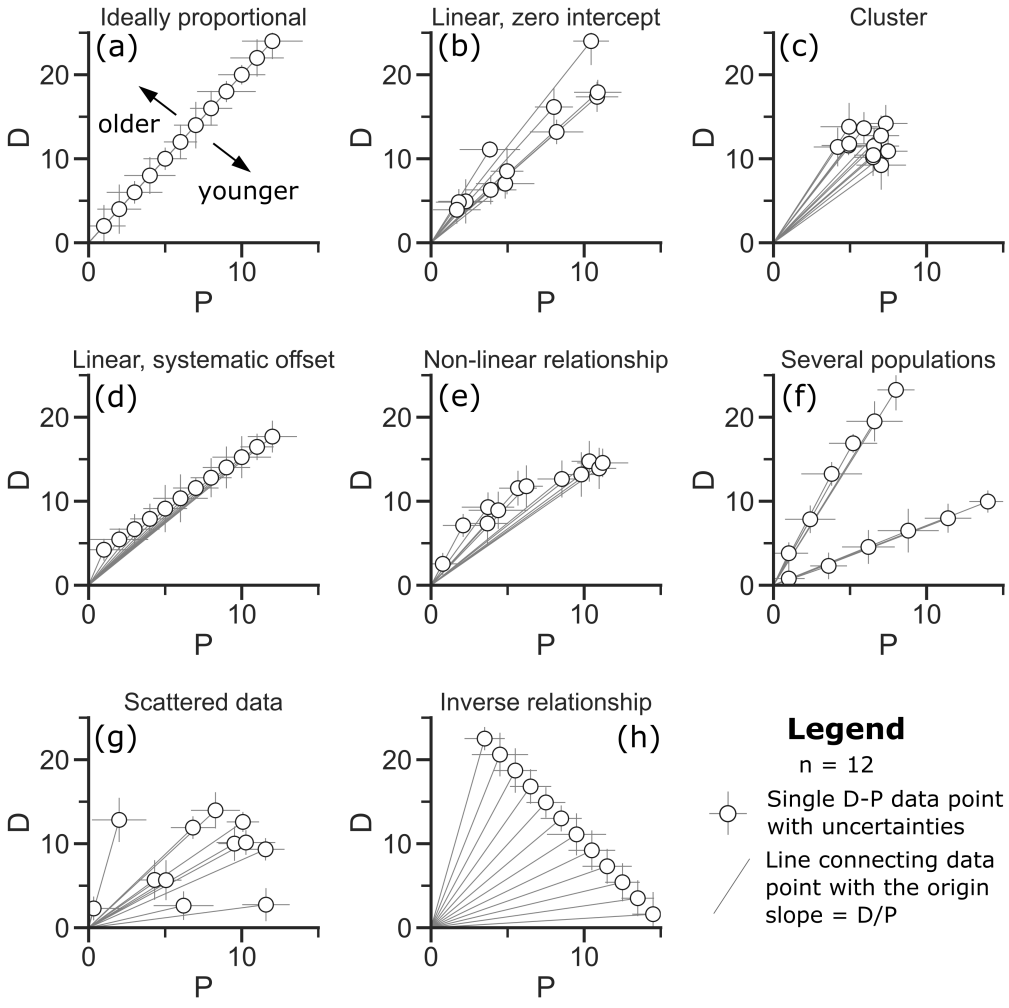

Figure 1. Synthetic data showing different daughter-parent relationships. Sect. 2.2 discusses the possible causes for data falling into each of these classes. Note, that the mean D/P ratio for each panel is 2.

In practice, the analyst acquires multiple single-grain data to determine a sample age. The number of these single-grain analyses varies between methods and analytical protocol – from about 20-30 grains per sample for FT and ZR dating to only 3 to 5 grains per sample for whole-grain He dating. The D-P plot allows us to analyze such multi-grain samples. In the ideal case data pairs from same-age grains plot on a line through the origin (Fig. 1a). However, real data deviate from this ideal trend. Figure 1b-h show synthetic data as examples for these deviations which can be summarized into seven classes. Their patterns may point to geological processes, analytical biases, or simply statistical outliers that need to be addressed during data analysis. Summarizing thermochronological ages by a sample mean age without examining the daughter-parent relationship thus does injustice to the data and may neglect important information. To illustrate that, the mean D/P ratio for

https://doi.org/10.5194/gchron-2024-1
Preprint. Discussion started: 25 January 2024

all the data in the panels of Fig. 1 is 2 – however, their appearance varies drastically. In addition, deviations from the ideal proportional relationship (Fig. 1a) create spurious correlations in age-(e)U plots (Chayes, 1949; Härtel et al., 2022a). In the following, we give a short overview of the shown classes of typical deviations from the ideal proportional D-P relationship.

Fig. 1b presents a positive linear D-P relationship with a zero intercept, including random variation about the trend. This is the ideal situation expected with uncertainty on the D and P measurements. Additional variation may be the consequence of varying grain sizes or inaccurate α-ejection correction for He dating, inter-grain chemical differences for FT or ZR dating, and parent-concentration-zoning for all three methods.

Fig. 1c shows clustering of D-P data. This pattern is typical for data from samples with limited inter-grain differences in parent (and daughter) concentrations, and usually their uncertainty intervals overlap strongly. In this case, the positive relationship between daughters and parents may be obscured by the data's uncertainty.

In Fig. 1d, the data form a linear trend as in Figs. 1a and b, but are offset from the origin. In He dating, such an offset may result from (1) 'parentless helium' implanted by inclusions (Vermeesch et al., 2007), or eU-bearing neighbors (e.g., Murray et al., 2014) or (2) a consistent style of zoning across grains affecting α-ejection correction (e.g., Orme et al., 2015). In FT dating, it may also be due to a bias towards higher or lower track counts. In ZR dating, systematic offsets may result from damage-calibration issues, asymmetric Raman bands, or composition-related Raman-band broadening (Troch et al., 2018; Härtel et al., 2021, 2022b). Note that an over- or underestimation of P causes an apparent offset of opposite sign in D.

Figure 1e showcases a non-linear relationship. This may be due to the daughter retention depending on the degree of lattice damage from α-decay of U, Th and their daughters. The production of radiation-damage is roughly proportional to the parent (eU) concentration. Its effect on daughter retention causes D and P to form either a concave (Fig. 1e, damage-enhanced loss) or a convex (damage-enhanced retention) relationship (Härtel et al., 2022a).

The data in Fig. 1f form two different trends, indicating different age components within the sample. This relationship may occur if a sample contains groups of grains with a high contrast in kinetic properties; an example for this are the high- and low-Cl apatite grains in the FT data of Stockli et al. (2001).

In Fig. 1g, random scatter obscures the relationship of D and P. Such a pattern can arise due to multiple reasons, e.g., heterogeneous daughter retention within the sample due to grain size, chemical composition, micro-cracks, deformation, or parent zoning, analytical reasons, such as inaccurate α-ejection correction or counting bias, or a combination of factors.

Figure 1h shows an inverse relationship between daughters and parents. This pattern may occur due to (1) the data representing a falling segment of a non-linear trend, (2) a small sample size causing a spurious relationship (Ketcham et al., 2018) or (3) bias from over- or under-correcting the He concentration for α-ejection.

Each of the shown relationships requires different considerations for data analysis. This includes the questions if reporting a single sample age is appropriate, and if yes, which type of sample age to report. In addition, the D-P plot allows to identify the relative position of outliers with respect to the rest of the data, showing if its main deviation occurs in D or P. It also helps to decide if a radiation-damage model is necessary to understand the geological history of the sample, and which other

https://doi.org/10.5194/gchron-2024-1
Preprint. Discussion started: 25 January 2024

data-analysis tools may provide further insights. Thus, the D-P plot contains essential information for translating data into time-temperature information.

Our ability to evaluate the D-P relationship for a sample clearly depends on the number of data. While this is not a concern for FT and ZR dating (n>10), it is a limiting factor for conventional whole-grain He dating (n<10). However, the recent development of laser ablation based He dating will increase the number of grains analyzed per sample and recognizing D-P relationships (e.g., Tripathy-Lang et al., 2013; Pickering et al., 2020). We discuss the limitations of D-P plots for small samples in sect. 4.1.

3 An analytical workflow based on D-P plot analysis

As Fig. 1 shows, the D-P plot provides a first step into thermochronological data analysis and helps to decide which analytical or geological factors may influence a dataset. We propose a decision-tree approach to classify the daughter-parent relationship (Fig. 2). Depending on the class of the relationship, it then suggests further steps of data analysis. The following sections outline the use of the decision tree to systematically classify the data and find an appropriate description of the contained thermal-history information.

3.1 Preliminary considerations

Before using the classification scheme in Fig. 2, it is essential to assure that the analytical procedures and samples meet certain quality criteria established for each method, e.g., that suitable grains were selected for He dating, that data with asymmetric Raman bands were excluded from ZR dating, that track counting was conducted on prismatic grain surfaces, etc. Also, the number of analyses in the dataset is important, as fitting a regression line or splitting a dataset into age populations is not appropriate for small datasets (see sect. 4.1). Another criterion to be considered is the geological background of the sample. For example, a crystalline bedrock sample with a simple cooling history will likely give a single age, while a metasedimentary rock may show different age populations due to chemical variation between grains, and a volcanic rock recording its eruption is expected to give a near-ideal linear trend. Radiation-damage effects and accompanying non-linear relationships are expected for old rocks with protracted or complex cooling histories, but not for young rocks that did not spend time in the temperature regime of radiation-damage accumulation. The interpretation of a sample that strongly deviates from the geological expectations needs to be carried out with care.

3.2 The classification procedure

For analyzing the data, we calculate the daughter and parent concentrations according to the thermochronological method used (see Appendix B) and plot them against each other. The analysis proceeds by following the decision tree in Fig. 2 to classify the daughter-parent relationship.

https://doi.org/10.5194/gchron-2024-1
Preprint. Discussion started: 25 January 2024

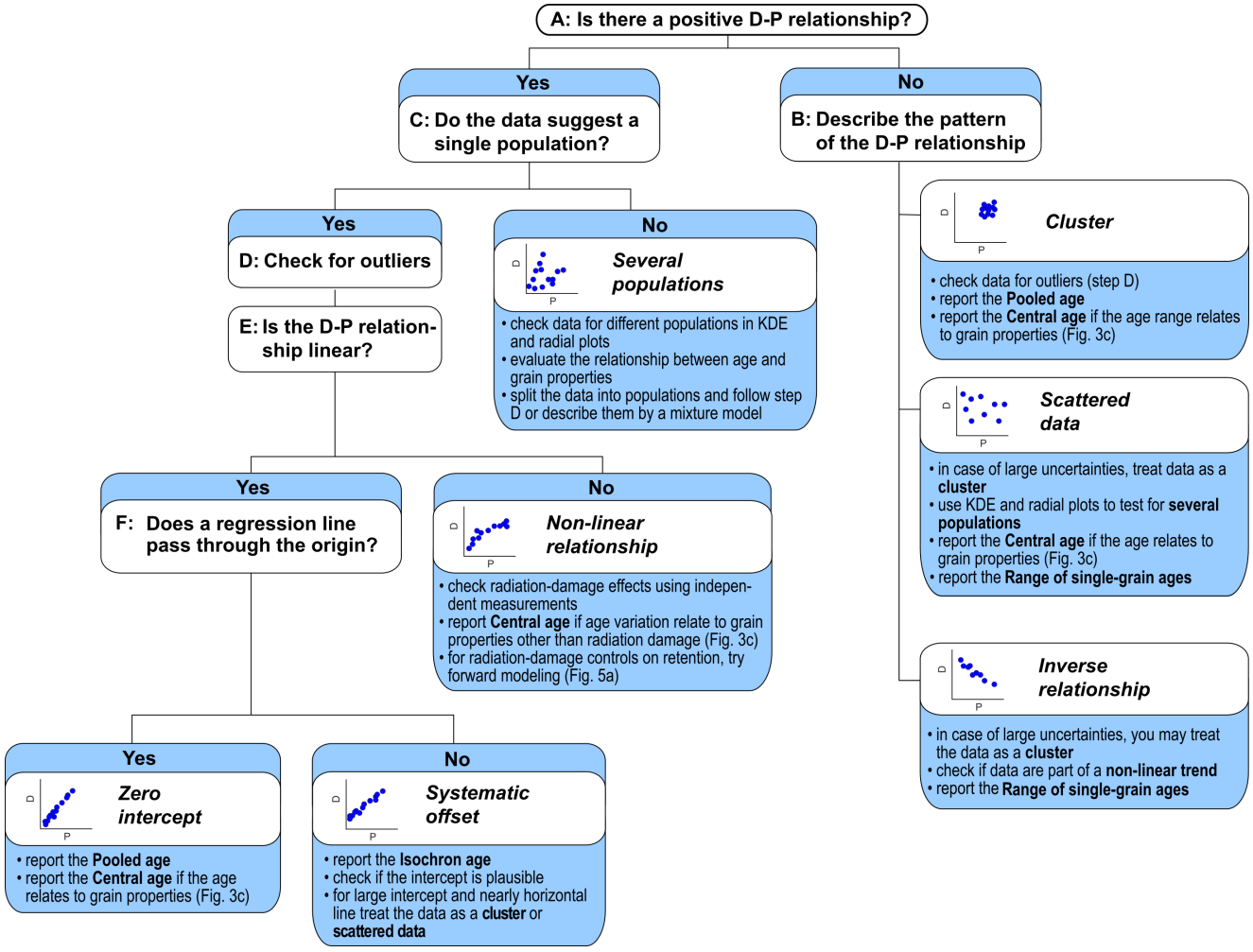

Figure 2. Flowchart for classifying the daughter-parent relationship in a sample (compare with Fig. 1). The blue boxes provide suggestions on how to treat data belonging to the respective class.

The first step separates datasets showing a positive D-P relationship from those that do not (A in Fig. 2). We expect a positive association between D and P from the radioactive production equation, but this association may be obscured by factors discussed in sect. 2.2. In the case of data for which the D-P relationship is not clear, it is usually safe to assume that there is no positive relationship – a decision that may be revised in later steps. Data, for which D and P are not positively associated, are then classified as either clustered, scattered or following an inverse relationship (B in Fig. 2; Fig. 1c, g, h).

For data with a positive D-P relationship, it is then essential to distinguish datasets containing a single age population from those with several populations (C in Fig. 2). As in Fig. 1f, multiple age populations form linear arrays with different slopes

https://doi.org/10.5194/gchron-2024-1
Preprint. Discussion started: 25 January 2024

or clusters in the dataset with gaps between them. A kernel-density-estimate (KDE) plot may reveal the presence of different populations for cases that are not clear-cut.

For single-population data, the next step is filtering the dataset for outliers (D in Fig. 2). Outliers stick out by a difference in single-grain age to the other data beyond their uncertainty. However, this is not sufficient evidence to mark a data pair as anomalous: other factors such as systematic offset may also cause single grains to be significantly older or younger than the others (Fig. 1d). In the D-P plot, outliers show up as removed from the main trend or group of data points. Before, considering such a measurement as anomalous, other properties should be examined, e.g. grain size or mineral chemistry. If anomalous data are excluded from further analysis, this should be reported, e.g. by marking the excluded data point as empty symbol in the D-P plot. For ambiguous cases, it may be advantageous to carry out the further steps with and without the concerned data point. For He dating, Flowers et al. (2022) provide further strategies for treating outliers (their sect. 3.1).

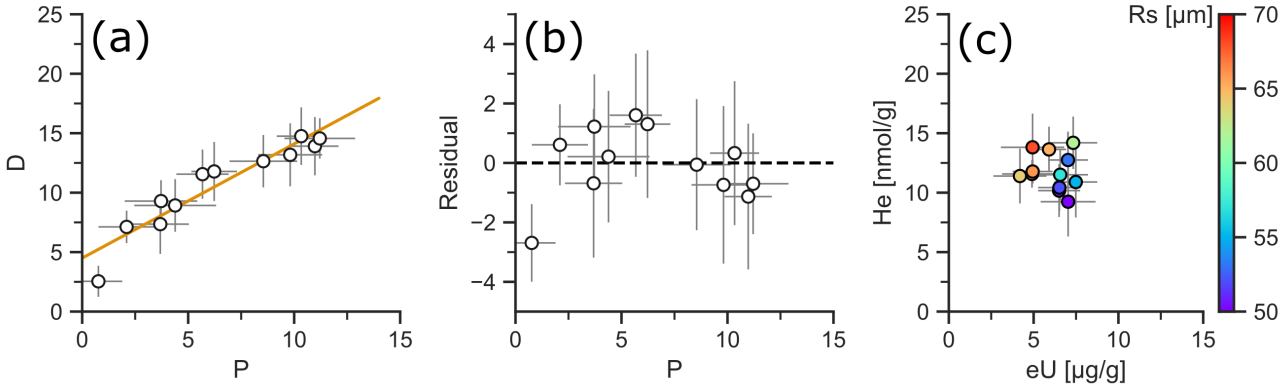

Figure 3. D-P plots for testing for a non-linear relationship and for age differences related to grain properties. (a) Regression line fit to a synthetic non-linear D-P relationship with the residuals (difference between measured and fitted D) shown in (b). (c) D-P plot for a synthetic He dataset showing a cluster relationship, color-coded by equivalent spherical radius (R_s).

After examining the outliers, we test the data for a linear D-P association (E in Fig. 2). If it is not clear whether the data show a linear or a non-linear trend from visual inspection alone, this can be verified by fitting a regression line to the data and examining the residuals, i.e. the deviation of the data points from the line. For a linear relationship, the residuals scatter randomly around zero while in the case of a non-linear relationship, there is an association between residual and parent concentration. Fig. 3a shows the linear fit to a synthetic dataset in a D-P plot. Figure 3b plots the fitting residuals against P, revealing a boomerang-shaped trend that points to a non-linear D-P relationship.

If the D-P relationship is linear, it is necessary to test the data for a systematic offset (F in Fig. 2). This is achieved by fitting a regression line to the data and examining its intercept. If the intercept includes zero in its uncertainty envelope, the offset is not significant and the data may be treated as having a zero intercept. If the uncertainty envelope does not include zero, this is a sign for a potential offset. However, this uncertainty on the intercept may be an underestimate if the variation of the data

https://doi.org/10.5194/gchron-2024-1
Preprint. Discussion started: 25 January 2024

strongly exceeds that expected from the uncertainties (e.g., high MSWD; Wendt and Carl, 1991; see Appendix C). Another simple test for an intercept is the comparison of the isochron age and the pooled age: if the data form a trend through the origin, the two ages should be indistinguishable because the pooled age assumes a zero intercept and should thus be indistinguishable from the isochron age (see sect. 3.3).

3.3 Classes of daughter-parent relationship

Once arrived at a certain class of D-P relationships, the goal is to assign an age to the sample. This can either be a central tendency, such as a mean or pooled age, or an isochron age for a sample with a single age population, or a number of ages or a range of single-grain age depending on the D-P relationship (Fig. 4, Table 1). If the given ages can be described by a single sample age, the simplest solution is to report a central tendency. Despite its simplicity, the (arithmetic) mean age does usually not provide a reliable sample age (e.g., Vermeesch, 2008; Härtel et al., 2022a). A more robust alternative is the pooled age, which uses the ratio of the summed D and P concentrations.

If the intra-sample age variation can be related to a certain grain property affecting radiogenic daughter retention, the ages may represent a continuous mixture, with each grain recording a different age due to its individual properties. Figure 3c shows an example with He data varying with respect to grain size. Such a mixture is best described by the central age (e.g. Galbraith, 2005; Vermeesch, 2019).

Datasets, that are systematically offset, require a different approach, that of the isochron age, which rests on the slope of a fitted regression line through the D-P data. If several discrete age components exist in a dataset, these can be separated by mixture modeling (e.g., Galbraith and Laslett, 1993; Vermeesch, 2019), or by treating each age component as a single sample.

If the data cannot be described by a single age or multiple ages, nor by a continuous mixture related to grain properties, it is still possible to report the range of single-grain ages, which does not rely on any model assumptions. Appendix C provides a more detailed discussion about mean and isochron ages, and discrete and continuous age mixtures. The following sections provide suggestions for how to treat data falling into each of the D-P classes of Fig. 2.

3.3.1 Linear relationship with zero intercept

If the daughter-parent relationship and the intercept of its regression line is close to zero (F in Fig. 2), the pooled and the isochron age are similar (Fig. 1b). In this case, it is advantageous to report the pooled age which is more robust and does not require the intercept as additional parameter. As all single-grain ages along the linear trend are roughly the same, the potential bias of the pooled age is negligible (see Appendix C).

If the MSWD or spine factor of the fitted regression line (F in Fig. 2) are outside the upper confidence limit, the data are over-dispersed. This points to two possible scenarios: (1) Analytical dispersion due to the uncertainties not reflecting the actual measurement error. This is especially a problem for He and laser-ablation FT dating (e.g., Fitzgerald et al., 2006; Ketcham et al., 2018; Cogné and Gallagher, 2021). In this case, the uncertainty on the pooled age may be expanded to take

https://doi.org/10.5194/gchron-2024-1
Preprint. Discussion started: 25 January 2024

into account the variation of the individual analyses (see Eq. (C6) in Appendix C). (2) Geological dispersion due to heterogeneous grain properties affecting daughter retention, such as grain size, composition etc. This can be tested by plotting the age against these properties, or by using them for color-coding the D-P plot (Fig. 3c). If the data are dispersed due to a continuous range of grain properties, the central age describes the age distribution best (Appendix C).

3.3.2 Cluster

Clustered data are best summarized by the pooled age (Fig. 1c). To make sure that there is no bias towards the oldest or highest-D-P grains, the data should be screened for outliers (D in Fig. 2). If the data are over-dispersed, e.g., failing the χ^2 test (e.g., Galbraith, 2005), the uncertainty of the pooled age may be expanded to reflect the actual inter-grain age variation (see Eq. (C6) in Appendix C). If there exists a relationship between age and grain properties, e.g. by plotting the age against these grain properties or to color-coding the D-P plot (Fig. 3c), the age distribution may be described by a central age.

3.3.3 Linear relationship with systematic offset

The only sample age that appropriately describes systematically offset data is the isochron age determined from the slope of a regression line (Appendix C). The intercept of the regression line provides a first-order estimate for the amount of offset, that may be interpretable in terms of 'parentless helium' or a systematic property of the analyzed grains. If the intercept is large, close to the mean daughter concentration, or if the data allow for a horizontal or vertical line fit, they could also be treated as a cluster (sect. 3.3.2) or scattered data (sect. 3.3.6). If the data are over-dispersed, e.g., showing an MSWD outside its confidence interval, it is possible to expand the uncertainty on the isochron age by multiplying it with $\sqrt{(MSWD)}$ (e.g., Ludwig, 2012). For a strong overdispersion (e.g., MSWD > 10), the data may also be treated as scattered (see sect. 3.3.6).

Systematically offset data pose a serious problem to many standard data analysis tools and should therefore be treated with caution: first, the offset causes spurious age-(e)U association (Härtel et al., 2022a) due to low-parent data points being more offset than high-parent ones (compare grey lines in Fig. 1d). Second, offset data will usually appear over-dispersed (and fail the χ^2 test) because the age deviations are usually not explained by the uncertainties. This complicates the use of radial plots, as the spread in single-grain ages may give way to an interpretation of ages as a mixture of discrete age components (see discussion in Vermeesch, 2019). In addition, this will hamper inverse thermal-history modeling, as the modeling algorithm will have to reconcile a large spread in ages without the uncertainties accounting for it (e.g., Vermeesch and Tian, 2014). As the offset affects each data point differently, this problem cannot be solved by expanding the uncertainties in D and P (Flowers et al., 2022a). Fourth, the use of log-ratios for data analysis as in the Helioplot (Vermeesch, 2010) is compromised because the offset disturbs all ratios derived from the D and P concentrations.

https://doi.org/10.5194/gchron-2024-1
Preprint. Discussion started: 25 January 2024

215 **3.3.4 Non-linear relationship**

A non-linear relationship in the D-P plot points to radiation-damage-dependent daughter retention. This assumption can be tested against independent radiation-damage measurements. Raman and infrared spectroscopy, or X-ray diffraction provide radiation-damage estimates for zircon or titanite (e.g., Nasdala et al., 1995; Deliens et al., 1977; Holland and Gottfried, 1955; Heller et al., 2019), while optical absorption spectroscopy or Raman spectroscopy are potential tools to measure radiation
220 damage in apatite (e.g., Ritter and Märk, 1984; Liu et al., 2008).

Alternatively, a non-linear D-P relationship could result from daughter retention depending on other grain properties and the different grains recording the same thermal history differently. This effect can be examined by plotting the age against these parameters or by color-coding the D-P plot (Fig. 3c). If such a relationship exists, the dataset may be described by a central age (see Appendix C).

225 If the decision for a non-linear versus a linear relationship with an offset is not clear (E in Fig. 2; Fig. 3a, b), the less complex linear model should be preferred over a non-linear model (sect. 3.3.3) in the absence of independent radiation-damage measurements.

For a non-linear trend caused by radiation-damage-dependent daughter retention, forward modeling of daughter and radiation-damage accumulation and annealing provides further insight into the thermal history (e.g., Flowers et al., 2009;
230 Willett et al., 2017; Guenthner et al., 2013). In this case, the D-P plot allows to compare the data to the D-P relationship predicted by the model. Figure 5a shows thermal-history forward models of Guenthner et al. (2013) for zircon He dating plotted as lines in comparison to the measured data.

3.3.5 Several populations

If the D-P plot suggests that several discrete age components are present in the sample, the KDE or radial plot are the
235 standard tools to examine the data. The occurrence of different components should also be tested for consistency, e.g., if a mixture of populations makes sense in the geological context (sect. 3.1). The age distribution can either be described by a mixing model (e.g., Galbraith and Laslett, 1993; Galbraith, 2005; Vermeesch, 2019) or by separating the data into age components to be analyzed individually according to the procedure in Fig. 2.

3.3.6 Scattered data

240 Data that vary strongly in age and are scattered in the D-P plot may result from several scenarios: First, they may be a consequence of underestimating the uncertainties with respect to the variation in the single-grain data (e.g., for He dating, Fitzgerald et al., 2006; Brown et al., 2013). Martin et al. (2023) and Zeigler et al. (2023) showed that especially the uncertainty related to α-ejection correction in whole-grain He dating is difficult to estimate, while α-ejection correction strongly contributes to the age error. Data with limited scatter, for which the uncertainties may be underestimated could be
245 treated as a cluster (sect. 3.3.2). A second explanation for scatter is the occurrence of different age populations, which can be

https://doi.org/10.5194/gchron-2024-1
Preprint. Discussion started: 25 January 2024

verified in a KDE plot and may be better observed within a larger dataset (sect. 3.3.5). Third, the scatter may also be due to each grain having slightly different daughter-retention properties and recording a different age. Plotting the age against these parameters or color-coding the D-P plot (Fig. 3c) allows to assess this relationship; a central age may be used to describe such a continuous mixture (sect. 3.3.2; Appendix C).

If the scatter cannot be explained by one of these scenarios, the range of the single grain ages should be reported. Scattered data also pose a serious problem to inverse t-T modeling, as the age difference may not allow for a single t-T path to reconcile the spread in ages.

3.3.7 Inverse relationship

An inverse daughter-parent relationship runs contrary to the relationship expected from the age equation (Fig. 1b). In general, while such data should be treated with caution, two scenarios can account for this relationship without pointing to a serious problem with the analyses in question. If the dataset is small (e.g., n≤5), a spurious inverse trend could arise randomly (Ketcham et al., 2018) and the dataset should be treated as scattered (sect. 3.3.6). However, the interpretation of small datasets should be carried out with caution (see sect. 4.1). Alternatively, the inverse relationship may represent an inverse segment of a non-linear trend, if daughter retention is affected by radiation damage (sect. 3.3.4; Fig. 5a). If there is no clear explanation for the inverse daughter-parent relationship, it is best to report the range of single-grain ages (Table 1; Appendix C).

3.4 Examples and reporting format

The above classification scheme allows for a clear path of decision to each of the D-P classes. Figure 4 shows three examples for daughter-parent plots, each with a different D-P relationship.

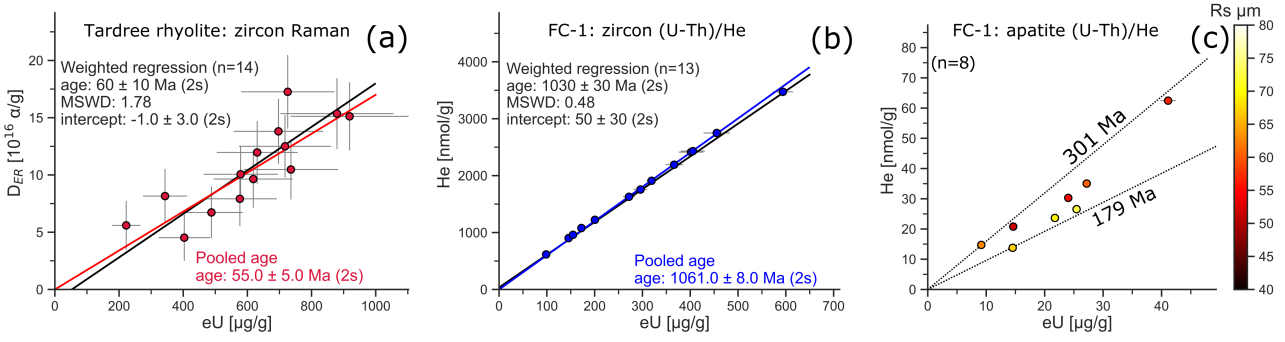

Figure 4. Examples for D-P plots. (a) ZR data of Tardree rhyolite (Härtel et al., 2021). (b) Whole-grain abraded ZHe data of Duluth Complex sample FC-1 (Härtel et al., 2023). (c) Whole-grain AHe data of Duluth Complex sample FC-1 (Härtel et al., 2023), color-coded by grain size. Solid black lines in (a) and (b) are fitted isochrons; colored lines represent the pooled age. The dotted lines in (c) denote the ages of the lowest- and highest-age grain, respectively.

https://doi.org/10.5194/gchron-2024-1
Preprint. Discussion started: 25 January 2024

The ZR data in Fig. 4a form a positive, linear relationship between radiation damage density D and eU. We classify the relationship as having a zero intercept, based on the intercept being within uncertainty of the origin (-1±3 10^{16} α/g; F in Fig. 2, sect. 3.2). The age to report in this case is the pooled age. Table 1 presents a reporting format for these data.

The ZHe data in Fig. 4b form a positive, linear relationship between He content and eU. However, there is a positive intercept (50±30 nmol/g) whose uncertainty envelope does not include the origin. We therefore classify the D-P relationship as linear with an offset and report the isochron age. The AHe data in Fig. 4c form a positive relationship, but they also exhibit much more variation than expected from their uncertainties and fitting a regression line to these data is difficult. We therefore classify the data as scattered. The color-coding by grain size shows that the variation in D and P cannot be explained as a consequence of grain size on He diffusion kinetics: the smaller grains contain more He compared to the larger grains. We therefore report the range of single-grain ages (179–301 Ma; Table 1).

Table 1. Example for reporting data-analysis results based on the D-P plots in Fig. 4.

Sample name	Dating method	D-P relationship	Age reported	Age (Ma)	n
TDR	ZR	Linear, zero intercept	Pooled age	55 ± 5	14
FC1	ZHe (whole grain, abraded)	Linear, offset	Isochron age	1030 ± 30	13
FC1	AHe (whole grain)	Scattered	Single-grain age range	179-301	8

4 Further considerations

4.1 Small datasets

While the classification with the flowchart in Fig. 2 is useful for larger datasets, it is important to point out its limitations for datasets consisting of few analyses. This concerns especially conventional whole-grain He dating, where sample sizes of ≤5 grains are common. There are several limits a small sample imposes on data analysis: (1) it is not possible to recognize different populations; (2) a single outlier may constitute a large proportion of the gathered data; (3) random variation may cause inverse D-P relationships (see Ketcham et al., 2018) or spurious associations between the age and other properties; (4) linear regression becomes useless due to the influence of single data on the regression fit. A classification following Fig. 2 is therefore not possible.

However, it is still possible to use the D-P plot as a qualitative guide, e.g., to visualize the data in terms of their variation in D and P. It also enables to examine in which D-P direction a potential outlier deviates from the rest of the data. This helps to decide whether a single data point with a different age may bias the pooled age (high D or P) or not (see Appendix C).

https://doi.org/10.5194/gchron-2024-1
Preprint. Discussion started: 25 January 2024

In terms of sample ages, the small number of grains inhibits the use of isochron or central ages, which would require the fitting of several parameters (age and intercept or dispersion) to a small amount of data. We therefore suggest using the pooled age or a range of ages.

4.2 Plotting multiple samples

An additional use for the D-P plot is the comparison of thermochronological data from different samples. This mode of analysis usually requires some geographical or geological context and thus belongs to a later step of the data analysis then the single-sample analysis. This data grouping hinges on the condition that the different samples are comparable, e.g., being geographically or geologically related. This strategy is often used for analyzing age-eU associations in apatite, zircon and titanite He dating (e.g., Guenthner et al., 2013; Baughman et al., 2017; Sturrock et al., 2021). Figure 5a shows grouped zircon He data from the Minnesota River (Miltich, 2005). While the D-P relationships differ strongly between samples, together, they form a non-linear trend that can in part be explained by radiation-damage-dependent He retention (models as lines; Guenthner et al., 2013; sect. 3.3.4).

It is also possible to group data from samples sharing a systematic difference in thermal history, e.g., those collected across a fault, or along an elevation profile or borehole. Comparing them in the D-P plot reveals their age pattern with respect to their position. Figure 5b shows zircon He data of Wolfe and Stockli (2010) from the Kontinentale Tiefbohrung (KTB) drillhole. The D-P plot highlights (1) the systematic difference in age between data from above and below 4 km depth, and (2) the variation in eU at different depths.

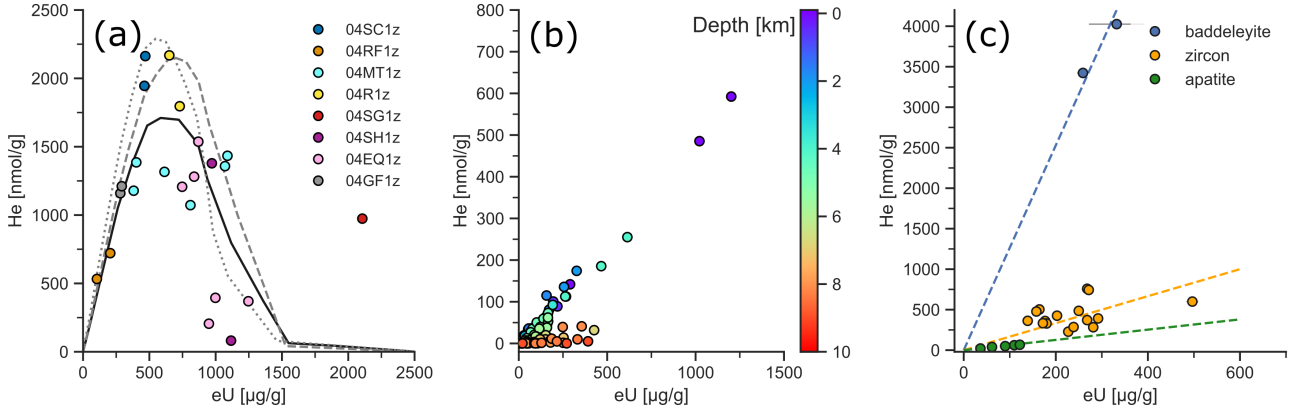

Figure 5. Examples of D-P plots comparing multiple samples. (a) D-P plot for the Minnesota-River zircon He dataset differentiated by sample (Miltich, 2005). The lines are zircon radiation-damage accumulation and annealing models comparing different thermal-history scenarios (dashed grey line: cooling at 0.17 °C/Ma since 1.8 Ga; dotted grey line: cooling at 0.13 °C/Ma; solid black line: acceleration of cooling at 1.1 Ga from 0.06 to 0.17 °C/Ma; models from Guenthner et al., 2013) for this dataset to compare different predictions to the measured data. (b) D-P plot for the Kontinentale Tiefbohrung (KTB) borehole zircon He data from Wolfe and Stockli (2010), color-coded by depth below the surface. (c) D-P plot comparing baddeleyite, zircon and apatite He data from the Phalaborwa Complex (Baughman and Flowers, 2018). Lines are guides for the eyes only.

https://doi.org/10.5194/gchron-2024-1
Preprint. Discussion started: 25 January 2024

Last but not least, the D-P enables us to compare the dating results for single samples across methods to: (1) examine age differences, (2) compare the D-P relationship, or (3) unexpected apparent age relationships, e.g. apatite FT-He age inversion (Green et al., 2006; Flowers and Kelley, 2011; Recanati et al., 2017). Figure 5c displays an example of apatite, baddeleyite and zircon He data from the Phalaborwa carbonatite complex, South Africa (Baughman and Flowers, 2018), showing the difference in helium retention and eU content between the three minerals.

4.3 Detrital samples

Detrital or sedimentary samples are more complicated than the cases shown here: they usually contain grains with different pre-depositional thermal histories, chemical composition and size. Therefore, extracting an age or an interpretation from a single sample or a single thermochronometer is usually not possible (e.g. Carter, 2019). Also, the versatility of detrital samples makes it difficult to trace an observed pattern in the D-P plot to its causes.

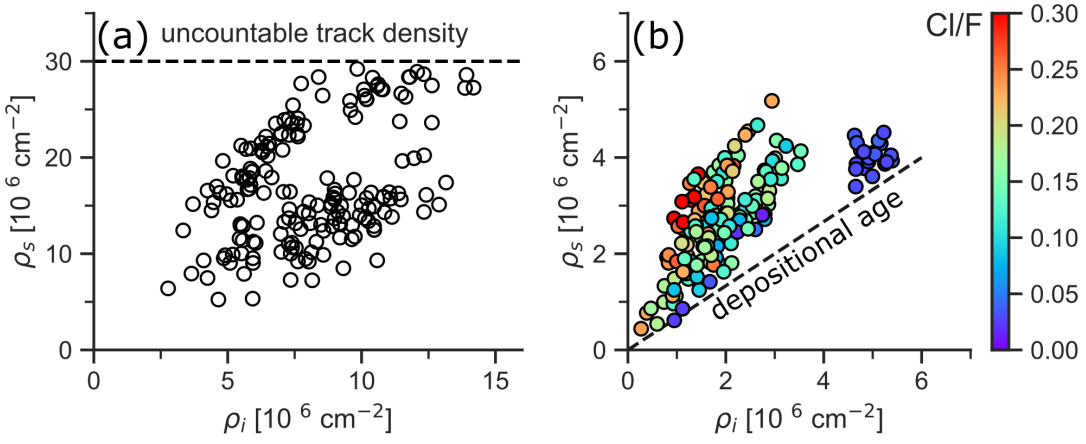

Figure 6. Possible applications for D-P plots for detrital thermochronology. (a) D-P plot for a synthetic ZFT dataset with the dashed line marking the density threshold, at which the spontaneous tracks become uncountable. (b) D-P plot for a synthetic AFT dataset color-coded by the Cl/F ratio. The dashed line represents the depositional age.

Standard procedures for interpreting detrital thermochronological data include identifying peak ages in the single-grain age distribution and putting them into the context of the stratigraphic age, age distributions of source areas, catchment geometry, etc. (e.g., Malusà and Fitzgerald, 2019). While it is possible to evaluate age distributions in the D-P plot (see sect. 3.3.5), KDE or radial plots are the more adequate tools for this. Still, the D-P plot may hold additional information that is difficult to access with these plots. First, it may be used on a subset of the data to evaluate the daughter-parent relationship for a given age peak and possibly detect a non-linear or systematically offset relationship (sect. 3.3.3, 3.3.4). However, this can only be done reliably, if enough data (e.g., n ≥10) are available in this grain population. Second, it may help to identify bias in grain selection. One of these is the problem with overlapping, uncountable fission tracks in old or U-rich zircon, that may skew

https://doi.org/10.5194/gchron-2024-1
Preprint. Discussion started: 25 January 2024

ZFT age populations towards younger ages and thus impact the interpretation in terms of source-area exhumation and erosion patterns (e.g., Malusà, 2019).

Figure 6a shows the D-P plot for a synthetic ZFT dataset. The dashed line marks the threshold uncountable spontaneous tracks. The countability limit cuts off the track-density distribution for an old grain population, and thereby indicates that the sample may contain older or higher-U grains not datable with the ZFT method. A third application is the visualization of different grain populations with respect to age, parent concentration and other grain properties, e.g. grain size or composition to highlight nuances in the composition of different age populations. Figure 6b shows the D-P plot for a synthetic AFT dataset with color-coding by the Cl/F ratio and a dashed line representing the depositional age. In this case, part of the grains in the age group slightly older than the depositional age, stands out due to its high induced-track density (high U content) and its halogen composition being dominated by fluorine. So, despite the complexity of detrital samples, there are situations, in which the visualization of the data in a D-P plot can be useful.

5 Conclusions

Plots of daughter vs. parent concentration (D-P plots) are a standard tool in radiometric dating representing a graphical solution of the age equation. D-P plots allow to identify sources of age variation, such as systematic offsets, outliers or the occurrence of several populations. We present a workflow that describes the use of D-P plots for thermochronological data analysis. Our approach follows a step-wise examination of the daughter-parent relationship and assigns one of seven classes to it. This enables us to choose the further steps for data analysis and identify possible factors influencing the age. The classification scheme is an attempt to make data analysis more consistent and transparent. It also enables thermochronologists to trace back the decisions made during data analysis. While there are limits of D-P plots dealing with small samples, the D-P plot provides many possibilities for comparing data across samples and thermochronometers, for detrital thermochronology and for analyzing data from newly developed dating methods or less routinely used mineral phases (e.g. hematite or baddeleyite He dating, ZR dating).

https://doi.org/10.5194/gchron-2024-1
Preprint. Discussion started: 25 January 2024

Appendix A: The effective uranium concentration

The effective uranium concentration (eU) summarizes the α-producing U, Th, and Sm concentrations to a common decay rate of U. The formulation of eU in Eq. (2) follows the equations in Härtel et al. (2021) and differs from other eU calculations, e.g. that of Shuster et al. (2006) or Cooperdock et al. (2019) in two regards: First, it recalculates the parent concentrations to the decay rate of ^{238}U instead of total U. This enables us to use eU as a single parent with a well-defined decay rate for He and ZR dating. Second, it takes into account the change of daughter production rate over geological time instead of using present-time production rates. Figure A1 shows how the normalization coefficients for each α-producing element change with respect to the age of a sample. The coefficients in Eq. (2) give accurate results for samples at ages <1000 Ma (Härtel et al., 2023), but may be modified if the expected ages for a set of samples are consistently higher or constrained well-enough to calculate them more accurately.

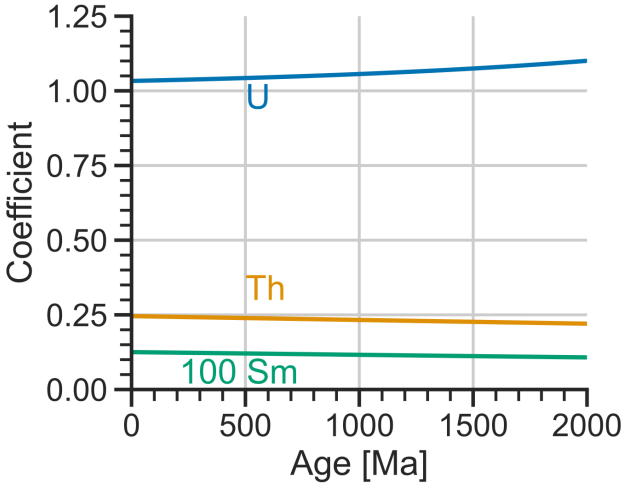

Fig. A1. Time-dependence of the coefficients for U, Th and Sm (multiplied by 100) in the eU equation (2).

The coefficients for eU are derived in Eq. (A1)-(A6). The starting point is the α-production equation:

$$N(\alpha) = 8\,\frac{N_A\left[{}^{238}U\right]}{M_{238}}\left(e^{\lambda_{238}t}-1\right) + 7\,\frac{N_A\left[{}^{235}U\right]}{M_{235}}\left(e^{\lambda_{235}t}-1\right) + 6\,\frac{N_A\left[{}^{232}Th\right]}{M_{232}}\left(e^{\lambda_{232}t}-1\right) + \frac{N_A\left[{}^{147}Sm\right]}{M_{147}}\left(e^{\lambda_{147}t}-1\right) \qquad \text{(A1)}.$$

N(α) is the number of alpha decays, N_A is the Avogadro constant, 8,7,6 and 1 are the numbers of alpha particle produced by the respective decay series, M are the molar masses, λ the decay constants and the symbols in brackets the concentrations (in units of mass) of each contributing parent nuclide. The constants used in the calculations are summarized in Table A1. Rescaling all summands to the terms of ^{238}U gives:

https://doi.org/10.5194/gchron-2024-1
Preprint. Discussion started: 25 January 2024

$$N(\alpha) = 8\,\frac{N_A}{M_{238}}\left(e^{\lambda_{238}t}-1\right)\left[\left(1+\frac{7}{8}\,\frac{M_{238}\left(e^{\lambda_{235}t}-1\right)}{M_{235}\left(e^{\lambda_{238}t}-1\right)}\,\frac{w_{235}}{w_{238}}\right)\left[{}^{238}U\right]+\left(\frac{6}{8}\,\frac{M_{238}\left(e^{\lambda_{232}t}-1\right)}{M_{232}\left(e^{\lambda_{238}t}-1\right)}\right)\left[{}^{232}Th\right]+\left(\frac{1}{8}\,\frac{M_{238}\left(e^{\lambda_{147}t}-1\right)}{M_{147}\left(e^{\lambda_{238}t}-1\right)}\right)\left[{}^{147}Sm\right]\right]$$

(A2).

eU is given by the term in the square brackets. For the elemental concentrations of the parents, this results in:

$$eU = \left[\left(1+\frac{7}{8}\,\frac{M_{238}\left(e^{\lambda_{235}t}-1\right)}{M_{235}\left(e^{\lambda_{238}t}-1\right)}\,\frac{w_{235}}{w_{238}}\right)[U]\,w_{238}+\left(\frac{6}{8}\,\frac{M_{238}\left(e^{\lambda_{232}t}-1\right)}{M_{232}\left(e^{\lambda_{238}t}-1\right)}\right)[Th]+\left(\frac{1}{8}\,\frac{M_{238}\left(e^{\lambda_{147}t}-1\right)}{M_{147}\left(e^{\lambda_{238}t}-1\right)}\right)[Sm]\,w_{147}\right] \quad \text{(A3).}$$

w_{235}, w_{238} and w_{147} are the mass fractions of the ^{235}U, ^{238}U and ^{147}Sm isotopes and the terms in square brackets are element concentrations. Equations (A4)-(A6) define the coefficients for each element:

$$k_U = w_{238}+\frac{7}{8}\,\frac{M_{238}\left(e^{\lambda_{235}t}-1\right)}{M_{235}\left(e^{\lambda_{238}t}-1\right)}\,w_{235} \quad \text{(A4),}$$

$$k_{Th} = \frac{6}{8}\,\frac{M_{238}\left(e^{\lambda_{232}t}-1\right)}{M_{232}\left(e^{\lambda_{238}t}-1\right)} \quad \text{(A5),}$$

$$k_{Sm} = \frac{1}{8}\,\frac{M_{238}\left(e^{\lambda_{147}t}-1\right)}{M_{147}\left(e^{\lambda_{238}t}-1\right)}\,w_{147} \quad \text{(A6).}$$

eU is then defined as:

$$eU = k_U[U]+k_{Th}[Th]+k_{Sm}[Sm] \quad \text{(A7),}$$

and the production equation simplifies to:

$$N(\alpha) = 8\,\frac{N_A}{M_{238}}\left(e^{\lambda_{238}t}-1\right)[eU] \quad \text{(A8).}$$

The time-dependence in Eq. (A4)-(A6) also allows iterative age calculation for He and ZR dating. This requires calculating eU from equation (A7) with a rough age estimate and then alternating between calculating the age from Eq. (1), and recalculating eU from Eq. (A4)-(A7) until the solutions converge.

https://doi.org/10.5194/gchron-2024-1
Preprint. Discussion started: 25 January 2024

Table A1. Coefficients and constants used in the calculations. The atomic masses and mass abundances are based on Holden et al. (2018), the decay constants are from Jaffey et al. (1971), Steiger and Jäger (1977), and Holden (1990). The decay constants are rounded to the first significant digit of their uncertainty.

Constant	Value
λ_{238}	$1.551\ 10^{-10}\ a^{-1}$
λ_{235}	$9.848\ 10^{-10}\ a^{-1}$
λ_{232}	$4.95\ 10^{-11}\ a^{-1}$
λ_{147}	$6.5\ 10^{-12}\ a^{-1}$
M_{238}	238.05 g/mol
M_{235}	235.04 g/mol
M_{232}	232.04 g/mol
M_{147}	146.91 g/mol
N_A	$6.022\ 10^{23}\ mol^{-1}$
w_{235}	0.0072
w_{238}	0.9928
w_{147}	0.1466

Appendix B: Units of daughter and parent concentrations

Daughter and parent concentrations can be expressed differently in external-detector-method FT and whole-grain He dating. Several criteria can be considered to find the right set of units for the D-P plot.

In He dating, the pairs of daughters (He) and parents (eU from U, Th, Sm) can either be expressed in units of abundance and mass (e.g., fmol and ng) or as concentrations (e.g., nmol/g and µg/g). The difference between these units is the normalization by the mass of the analyzed grain. For non-normalized data, the size or mass of the analyzed grains will introduce variation into D and P that is unrelated to the age of the sample. In case the grains differ strongly in size, this may bias the pooled age towards the largest grains and the isochron age towards the smallest or the largest ones (see Appendix C). Rescaling the units of D and P to concentrations eliminates this potential bias. Furthermore, it is advantageous to correct the He concentration for α-ejection correction before calculating the age: correcting for α-ejection after age calculation introduces a positive bias to the age (e.g., Vermeesch, 2008). Therefore, the corrected He concentration should be used as daughter concentration for plotting. In external-detector FT dating, a similar question of units arises concerning the use of either the spontaneous- and

https://doi.org/10.5194/gchron-2024-1
Preprint. Discussion started: 25 January 2024

induced-track counts or their track densities. In this case, it is advantageous to use the track densities instead of the counts to avoid bias towards big grains.

The specific units then determine the value of the constant c in Eq. (1). Re-arranging it to a daughter-production equation gives:

$$D = \frac{1}{c}\left(e^{\lambda t} - 1\right)[P] \quad \text{(B1)}.$$

For ZR dating, c results from equating Eq. (B1) and (A8):

$$c = \frac{M_{238}}{8\ N_A} = 4.94\ 10^{-23}\ g/\alpha \quad \text{(B2)}.$$

Given input damage densities in 10^{16} α/g and eU concentrations in µg/g, c takes a value of 0.494 [10^{-16} µg/α].

For He dating, the same relationship as for ZR dating applies, with the difference of He concentrations usually being reported in molar concentrations:

$$c = \frac{M_{238}}{8} = 29.76\ g/mol \quad \text{(B3)}.$$

If the input He concentrations are in in nmol/g and the eU concentrations in µg/g, c takes a value of 0.02976 [µg/nmol].

For FT dating, the constant c depends on measured experimental factors. This gives:

$$c = 0.5\ \lambda_D\ \zeta\ \rho_D \quad \text{(B4)}$$

for the external detector method, where 0.5 is the geometry factor, λ_D is the total decay constant for ^{238}U, ζ is the proportionality factor determined from dating an age reference material, and ρ_D the dosimeter track density (see Hurford, 2019). In this case, c is dimensionless because the spontaneous and induced-track counts densities are expressed in the same measurement units.

Laser-ablation FT dating requires a slightly different value for c because no dosimeter glass is involved in parent measurement (see Vermeesch, 2019):

$$c = 0.5\ \lambda_D\ \zeta \quad \text{(B5)}.$$

In this case, the dimension of c depends on the units of parent measurement, e.g. as U concentration or as element ratio, e.g., U/Ca.

https://doi.org/10.5194/gchron-2024-1
Preprint. Discussion started: 25 January 2024

Appendix C: Age calculation and reporting

C1 Mean ages

For datasets showing a single age, it is attractive to report the arithmetic mean age due to its familiarity and simple calculation. However, the mean age is inadequate for summarizing most thermochronological ages. First, calculating a mean from ages determined by a logarithmic age equation as in (1) 'linearizes' the age equation and causes a negative bias compared to applying the logarithmic age equation to a mean D/P ratio. Second, even when directly applied to the ratio, the arithmetic mean gives a biased age estimate, as can be shown from its relationship to the pooled age (see below; Pearson, 1896; Härtel et al., 2022a):

$$t_{mean} = t_{pooled}\left(1 - r_{DP}\, v_P\, v_D + v_P{}^2\right) \quad \text{(C1)}.$$

v_D and v_P are the variation coefficients (standard deviation divided by arithmetic mean) of the daughter and parent concentrations, and r_{DP} is their correlation coefficient. Equation (C1) shows that for the ideal proportional D-P relationship (r_{DP} = 1, v_D = v_P), the mean and pooled ages are the same. In a less ideal case, the measurement error on the parent concentration increases v_P and – as it is independent of the daughter concentration – weaken the relationship between D and P (decreasing r_{DP}). This causes the mean age to increase with respect to the pooled age. It means that the mean age is biased towards higher ages under non-ideal daughter-parent relationships. This is especially problematic for the whole-grain He and laser-ablation FT methods, for which the analytical uncertainties are often too small to explain the observed age variation (e.g., Fitzgerald et al., 2006; Ketcham et al., 2018). Essentially, measurement error on the parent concentration creates a right-skewed age distribution, whose mean increases with increasing variance and is biased towards higher ages.

A more robust alternative for calculating a central tendency is the pooled age, i.e., treating all analyzed grains as a single grain by summing up all daughter and parent concentrations. The age is then calculated by substituting the ratio of these sums for D/P in Eq. (1):

$$t_{pooled} = \frac{1}{\lambda}\ln\left(1 + c\,\frac{\sum D}{\sum P}\right) \quad \text{(C2)}.$$

Vermeesch (2008) pointed out that in the presence of outliers with high parent concentration or age, the pooled age is biased towards these grains. Also, Green (1981) and Galbraith and Laslett (1993) argued that the pooled age is not appropriate as sample age, if the age variation cannot be explained by the estimated uncertainties. However, in the case of clustered data (sect. 3.3.2) or those forming a linear trend with zero intercept (sect. 3.3.1) without outliers, the age variation is small so that the bias on the pooled age can be assumed to be negligible. The uncertainty on the pooled age can be estimated from error propagation of the single-grain uncertainties. For He and ZR dating, this gives:

$$s\left(t_{pooled}\right) = t_{pooled}\sqrt{\frac{\sum s\left(D\right)^2}{\left(\sum D\right)^2} + \frac{\sum s\left(P\right)^2}{\left(\sum P\right)^2}} \quad \text{(C3)},$$

https://doi.org/10.5194/gchron-2024-1
Preprint. Discussion started: 25 January 2024

with s representing the uncertainties on D, P, and t, respectively. FT dating requires to also take into account the uncertainty on c (see Eq. (B4) and (B5)) in Eq. (C2). For the EDM method, this gives (Galbraith, 2005):

$$s\left(t_{pooled}\right) = t_{pooled}\sqrt{\left(\frac{s\left(\zeta\right)}{\left(\zeta\right)}\right)^2 + \frac{1}{\sum N_s} + \frac{1}{\sum N_i} + \frac{1}{\sum N_d}} \qquad \text{(C4)}.$$

N_s, N_i and N_d are the spontaneous, induced, and dosimeter track counts, respectively; ζ and s(ζ) are the calibration factor and its uncertainty.

For laser-ablation FT dating, the uncertainty on the pooled age is:

$$s\left(t_{pooled}\right) = t_{pooled}\sqrt{\left(\frac{s\left(\zeta\right)}{\left(\zeta\right)}\right)^2 + \frac{1}{\sum N_s} + \frac{\sum s\left(P\right)^2}{\left(\sum P\right)^2}} \qquad \text{(C5)}.$$

If the ages from a dataset are over-dispersed due to the uncertainties not reflecting the variation in the data, it may be advantageous to estimate the uncertainty of the pooled age directly from the variation in D and P concentrations (e.g., Pearson, 1896):

$$s\left(t\right) = t\sqrt{\frac{v_D^2 + v_P^2 - r_{DP}\, v_D\, v_P}{n}} \qquad \text{(C6)}.$$

v_D and v_P represent the variation coefficients of D and P, and r_{DP} is the correlation coefficient for the D-P relationship. Equation (C6) may give a more realistic uncertainty estimate than those in Eq. (C3)-(C5) if the data are slightly over-dispersed. For strongly scattered data, however, (C6) gives a large uncertainty, confirming that a single sample age may be meaningless.

C2 Isochron ages

For systematically offset data (sect. 3.3.3), the single-grain ages and the pooled age are offset in the same direction and give erroneously high or low ages. In this case, it is advantageous to calculate an isochron age by fitting a regression line to the D-P data and replacing D/P in Eq. (1) by the slope m:

$$t_{isochron} = \frac{1}{\lambda}\ln\left(1 + cm\right) \qquad \text{(C7)}.$$

The uncertainty on the isochron age results from propagation of the slope's uncertainty. This logarithmic age equation avoids the bias of the isochron age identified by Vermeesch (2008) for a linear age equation.

Typical algorithms for fitting isochrons are uncertainty-weighted (York, 1968; Kullerud, 1991) and robust regression (Huber, 1981; Powell et al., 2020). Both of these assign weights to each data point: the former based on the measured uncertainty, the latter based on the uncertainty and the distance of each point from a linear 'spine' in the data. Robust regression is therefore useful for datasets in which single grains fall off well-defined trends. However, its benefits are limited in the case of many grains deviating from the trend.

https://doi.org/10.5194/gchron-2024-1
Preprint. Discussion started: 25 January 2024

In general, data at the low- and high-parent ends of the distribution and data with small uncertainties have a strong influence on the isochron age, making it sensitive for outliers. Its use should therefore be limited to cases of systematic offset in the D-P relationship. Apart from the isochron age, the intercept may also contain important information for the interpretation and should be reported together with the age (sect. 3.3.3).

The mean square weighted deviation (MSWD; or the spine width for robust isochrons) of the isochron provides information on how well the isochron fits the data. An MSWD within the confidence interval (Table C1) indicates that the variation of the data about the isochron is within the range expected from the input uncertainties A high MSWD outside the confidence interval (Table C1) denotes over-dispersed data, whose variation is not explained by the input uncertainties alone – this may either point to unidentified sources of error or inter-grain variation of true ages within a sample. For He and laser-ablation FT data, whose sources of error are not yet well understood, these metrics have to be used with caution.

A standard practice to account for over-dispersed data in geochronology is to expand the uncertainty of the isochron age, multiplying it by $\sqrt{MSWD}$ (e.g., Ludwig, 2012).

Table C1. Confidence intervals (95 %) for the MSWD and the spine width for isochron fits (n-2 degrees of freedom). The MSWD intervals are based on Wendt and Carl (1991), the intervals for the spine width are from Powell et al. (2020).

	MSWD		Spine width	
n	Lower boundary	Upper boundary	Lower boundary	Upper boundary
10	0.50	2.00	0.31	1.55
15	0.61	1.78	0.4	1.5
30	0.73	1.53	0.58	1.39
60	0.81	1.37	0.71	1.28

C3 Age mixtures

Apart from the simple cases, discrete or continuous mixtures of ages may occur. There are two strategies to deal with discrete age components in a sample (sect. 3.3.5): mixture modeling (e.g., Galbraith and Laslett, 1993; Galbraith, 2005; Vermeesch, 2019), or splitting the data into different groups and calculating sample ages for each of them.

A continuous age mixture occurs if a sample contains grains with a wide range of kinetic properties responding differently to same thermal history (e.g., Vermeesch, 2019) – each grain then acts as single thermochronometer. An example could be the apatite FT age in a monotonously cooled plutonic rock with grains of different Cl/F ratio. In this case, the intra-sample age variation reflects both, the measurement error and the true-age variation between grains. This distribution is best described by a 'random effects model' and the age to be reported is the central age (Galbraith and Laslett, 1993) – the dispersion parameter describes the variation in true ages. Note however, that it is necessary to relate the single-grain age to a kinetic

https://doi.org/10.5194/gchron-2024-1
Preprint. Discussion started: 25 January 2024

parameter such as grain size, mineral chemistry, or measured radiation damage (Fig. 3c) to justify the use of a continuous mixture of ages. Galbraith (2005) and Vermeesch (2019) provide further discussion and calculation algorithms of the central age for FT dating, and Vermeesch (2008) for He dating. For complex data that cannot be described by a discrete or continuous mixture, we suggest to report the range of single-grain ages, which requires no additional assumptions.

Data availability

There were no new data produced for this manuscript other than the synthetic data shown in some of the Figures.

Author contribution

BH: Conceptualization, Methodology, Formal analysis, Visualization Writing – original draft preparation; EE: Conceptualization, Visualization, Funding acquisition, Writing – review and editing.

Competing interests

The authors declare that they have no conflict of interest.

Acknowledgements and Funding

This research was funded by the Natural Sciences and Engineering Research Council of Canada (NSERC) RGPIN-2018-03932 (Eva Enkelmann) and the University of Calgary Eyes High postdoctoral match funding to Birk Härtel.

References

Baughman, J.S., and Flowers, R.M.: Deciphering a 2 Gyr-long thermal history from a multichronometer (U-Th)/He study of the Phalaborwa carbonatite, Kaapvaal craton, South Africa, Geochem., Geophys., Geosys, 19, 1581–1594, https://doi.org/10.1029/2017GC007198, 2018.

Baughman, J., Flowers, R.M., Metcalf, J.R. and Dhansay, T.: Influence of radiation damage on titanite He diffusion kinetics, Geochim. Cosmochim. Acta, 205, 50-64, https://doi.org/10.1016/j.gca.2017.01.049, 2017.

Brown, R.W., Beucher, R., Roper, S., Persano, C., Stuart, F., and Fitzgerald, P.: Natural age dispersion arising from the analysis of broken crystals. Part I: Theoretical basis and implications for the apatite (U–Th)/He thermochronometer, Geochim. Cosmochim. Acta, 122, 478-497, http://dx.doi.org/10.1016/j.gca.2013.05.041, 2013.

Carter, A.: Thermochronology on sand and sandstones for stratigraphic and provenance studies, in: Fission-track thermochronology and its application to Geology, edited by: Malusà, M.G., and Fitzgerald, P.G., Springer International Publishing, New York, pp. 259-268, https://doi.org/10.1007/978-3-319-89421-8_14, 2019.

Chayes, F.: On ratio correlation in petrography, J. Geol., 57, 239-254, 1949.

Cooperdock, E.H.G., Ketcham, R.A., and Stockli, D.F.: Resolving the effects of 2-D versus 3-D grain measurements on apatite (U-Th)/He age data and reproducibility, Geochronology, 1, 17-41, https://doi.org/10.5194/gchron-1-17-2019, 2019.

Cogné, N., and Gallagher, K.: Some comments on the effect of uranium zonation on fission track dating by LA-ICP-MS, Chem. Geol., 573, 120226, https://doi.org/10.1016/j.chemgeo.2021.120226, 2021.

Deliens, M., Delhal, J., and Tarte, P.: Metamictization and U-Pb systematics – a study by infrared absorption spectrometry of Precambrian zircons, Earth Planet. Sci. Lett., 33, 331-344, https://doi.org/10.1016/0012-821X(77)90085-1, 1977.

Dunkl, I.: Trackkey: a Windows program for calculation and graphical presentation of fission track data, Comput. Geosci., https://doi.org/10.1016/S0098-3004(01)00024-3, 28. 3-12, 2002.

Fitzgerald, P.G., Baldwin, S.L., Webb, L.E., and O'Sullivan, P.B.: Interpretation of (U-Th)/He single grain ages from slowly cooled crustal terranes: a case study from the Transantarctic Mountains of southern Victoria Land, Chem. Geol., 225, 91-120, https://doi.org/10.1016/j.chemgeo.2005.09.001, 2006.

Flowers, R.M., and Kelley, S.A.: Interpreting data dispersion and "inverted" dates in apatite (U-Th)/He and fission-track datasets: An example from the US midcontinent, Geochim. Cosmochim. Acta, 75, 5169-5186, https://doi.org/10.1016/j.gca.2011.06.016, 2011.

Flowers, R.M., Ketcham, R.A., Shuster, D.L., and Farley, K.A.: Apatite (U-Th)/He thermochronometry using a radiation damage accumulation and annealing model, Geochim. Cosmochim. Acta, 73, 2347-2365, https://doi.org/10.1016/j.gca.2009.01.015, 2009.

Flowers, R.M., Ketcham, R.A., Enkelmann, E., Gautheron, C., Reiners, P.W., Metcalf, J.R., Danišik, M., Stockli, D.F., and Brown, R.W.: (U-Th)/He chronology: Part 2. Considerations for evaluating, integrating, and interpreting conventional individual aliquot data, Geol. Soc. Am. Bull., 135, 137-161, https://doi.org/10.1130/B36268.1, 2022.

Galbraith R.F.: Statistics for fission track analysis, Chapman & Hall, Boca Raton, Florida, 219 pp., ISBN: 9780367392796, 2005.

Galbraith, R.F., and Laslett, G.M.: Statistical models for mixed fission track ages, Nucl. Tracks Radiat. Meas., 21, 459-470, https://doi.org/10.1016/1359-0189(93)90185-C, 1993.

Green, P.F.: A new look at statistics in fission-track dating, Nucl. Tracks, 55, 77-86, https://doi.org/10.1016/0191-278X(81)90029-9, 1981.

https://doi.org/10.5194/gchron-2024-1
Preprint. Discussion started: 25 January 2024

Green, P.F., Crowhurst, P.V., Duddy, I.R., Japsen, P., and Holford, S.P.: Conflicting (U-Th)/He and fission track ages in apatite: Enhanced He retention, not anomalous annealing behaviour, Earth Planet. Sci. Lett., 250, 407-427, https://doi.org/10.1016/j.epsl.2006.08.022, 2006.

Guenthner, W.R., Reiners, P.W., Ketcham, R.A., Nasdala, L., and Giester, G.: Helium diffusion in natural zircon: Radiation damage, anisotropy, and the interpretation of (U-Th)/He thermochronology, Am. J. Sci., 313, 145-198, https://doi.org/10.2475/03.2013.01, 2013.

Härtel, B., Jonckheere, R., Wauschkuhn, B., Hofmann, M., Frölich, S., and Ratschbacher, L.: Zircon Raman dating: Age equation and calibration, Chem. Geol., 579, 120351, https://doi.org/10.1016/j.chemgeo.2021.120351, 2021

Härtel, B., Jonckheere, R., Krause, J., and Ratschbacher, L.: Spurious age-eU associations in thermochronology, Earth Planet. Sci. Lett., 117870, https://doi.org/10.1016/j.epsl.2022.117870, 2022a.

Härtel, B., Jonckheere, R., and Ratschbacher, L.: Multi-band Raman analysis of radiation damage in zircon for thermochronology: Partial annealing and mixed signals, Geochem. Geophys. Geosys., 23, e2021GC010182, https://doi.org/10.1029/2021GC010182, 2022b.

Härtel, B., Matthews, W.A., and Enkelmann, E.: Duluth Complex FC1 apatite and zircon: reference materials for (U-Th)/He dating? Geostand. Geoanal. Res., 47, 669-681, https://doi.org/10.1111/ggr.12492, 2023.

Heller, B.M., Lünsdorf, N.K., Dunkl, I., Molnár, F., and von Eynatten, H.: Estimation of radiation damage in titanites using Raman spectroscopy, Am. Min., 104, 857-868, https://doi.org/10.2138/am-2019-6681, 2019.

Holden, N.E.: Total half-lives for selected nuclides, Pure Appl. Chem., 62, 941-958, https://doi.org/10.1351/pac199062050941, 1990.

Holden, N.E., Coplen, T.B., Böhlke, J.K., Tarbox, L.V., Benefield, J., de Laeter, J.R., Mahaffy, P.G., O`Connor, G., Roth, E., Tepper, D.H., Walczyk, T., Wieser, M.E., and Yoneda, S.: IUPAC periodic table of the elements and isotopes (IPTEI) for the education community, Pure Appl. Chem., 90, 1833-2092, https://doi.org/10.1515/pac-2015-0703, 2018.

Holland, H.D., and Gottfried, D.: The effect of nuclear radiation on the structure of zircon, Acta Crystallogr., 8, 291-300, https://doi.org/10.1107/S0365110X55000947, 1955.

Huber, P.J.: Robust Statistics, John Wiley and Sons, Inc., New York, 305 pp., https://doi.org/10.1002/9780470434697, 1981.

Hurford, A.J.: An historical perspective on fission-track thermochronology, in: Fission-track thermochronology and its application to Geology, edited by: Malusà, M.G., and Fitzgerald, P.G., Springer International Publishing, New York, pp. 3-24, https://doi.org/10.1007/978-3-319-89421-8_1, 2019.

Jaffey, A.H., Flynn, K.F., Glendenin, L.E., Bentley, W.C., and Essling, A.M.: Precision measurement of half-lives and specific activities of 235U and 238U, Phys. Rev. C, 4, 1889-1906, https://doi.org/10.1103/PhysRevC.4.1889, 1971.

Ketcham, R.A., van der Beek, P., Barbarand, J., Bernet, M., and Gautheron, C.: Reproducibility of Thermal History Reconstruction from Apatite Fission-Track and (U-Th)/He Data, Geochem. Geophys. Geosys., 19, 2411–2436, https://doi.org/10.1029/2018GC007555, 2018.

Kullerud, L.: On the calculation of isochrons, Chem. Geol., 87, 115-124, https://doi.org/10.1016/0168-9622(91)90045-X, 1991.

Kulp, J. L., Volchok, H. L., and Holland, H. D.: Age from metamict minerals, Am. Min., 37, 709-718, 1952.

Li, Y., and Vermeesch, P.: Short communication: Inverse isochron regression for Re–Os, K–Ca and other chronometers, Geochronology, 3, 415-420, https://doi.org/10.5194/gchron-3-415-2021, 2021.

Liu, J., Glasmacher, U.A., Lang, M., Trautmann, C., Voss, K.-O., Neumann, R., Wagner, G. A., and Miletich, R.: Raman spectroscopy of apatite irradiated with swift heavy ions with and without simultaneous exertion of high pressure, Appl. Phys. A, 91, 17-22, https://doi.org/10.1007/s00339-008-4402-9, 2008.

Ludwig, K.R.: Isoplot/Ex Version 3.75: A geochronological toolkit for Microsoft Excel, Special Publication, 4, Berkeley Geochronology Center, 1-75, 2012.

Malusà, M.G.: A guide for interpreting complex detrital age patterns in stratigraphic sequences, in: Fission-track thermochronology and its application to Geology, edited by: Malusà, M.G., and Fitzgerald, P.G., Springer International Publishing, New York, pp. 279-293, https://doi.org/10.1007/978-3-319-89421-8_16, 2019.

Malusà, M.G., and Fitzgerald, P.G.: Application of thermochronology to geologic problems: bedrock and detrital approaches, in: Fission-track thermochronology and its application to Geology, edited by: Malusà, M.G., and Fitzgerald, P.G., Springer International Publishing, New York, pp. 191-209, https://doi.org/10.1007/978-3-319-89421-8_10, 2019.

Martin, P.E., Metcalf, J.R., and Flowers, R.M.: Calculation of uncertainty in the (U-Th)/He system, Geochronology, 5, 91-107, https://doi.org/10.5194/gchron-5-91-2023, 2023.

Miltich, L.: Low temperature cooling history of Archean gneisses and Paleoproterozic granites of southwestern Minnesota, B.A. thesis, Carleton College, Minnesota, 58 pp, 2005.

Murray, K.E., Orme, D.A., and Reiners, P.W.: Effects of U-Th-rich grain boundary phases on apatite helium ages, Chem. Geol., 390, 135-151, https://doi.org/10.1016/j.chemgeo.2014.09.023, 2014.

Nasdala, L., Irmer, G., and Wolf, D.: The degree of metamictization in zircon: A Raman spectroscopic study, Eur. J. Min., 7, 471-478, 1995.

Nasdala, L., Wenzel, M., Vavra, G., Irmer, G., and Kober, B.: Metamictisation of natural zircon: accumulation versus thermal annealing of radioactivity-induced damage, Contrib. Min. Petrol., 141, 125-144, https://doi.org/10.1007/s004100000235, 2001.

Nicolaysen, L.O.: Graphic interpretation of discordant age measurements on metamorphic rocks, Ann. N. Y. Acad. Sci., 91, 198-206, https://doi.org/10.1111/j.1749-6632.1961.tb35452.x, 1961.

Orme, D.A., Reiners, P.W., Hourigan, J.K., and Carrapa, B.: Effects on inherited cores and magmatic overgrowths on zircon (U-Th)/He ages and age-eU trends from Greater Himalayan sequence rocks, Mount Everest region, Tibet, Geochem. Geophys. Geosys., 16, 2499-2507, https://doi.org/10.1002/2015GC005818, 2015.

Pearson, K.: Mathematical contribution to the theory of evolution. On a form of spurious correlation which may arise when indices are used in the measurement of organs, Proc. R. Soc. Lond., 60, 489-498, 1896.

Pickering, J., Matthews, W.A., Enkelmann, E., Guest, B., Sykes, C., and Koblinger, B.M.: Laser ablation (U-Th-Sm)/He dating of detrital apatite, Chem. Geol., 548, 119683, https://doi.org/10.1016/j.chemgeo.2020.119683, 2020.

Powell, R., Green, E.C.R., Marillo Sialer, E., and Woodhead, J.: Robust isochron calculation, Geochronology, 2, 325-342, https://doi.org/10.5194/gchron-2-325-2020, 2020.

Recanati, A., Gautheron, C., Barbarand, J., Missenard, Y., Pinna-Jamme, R., Tassan-Got, L., Carter, A., Douville, E., Bordier, L., Pagel, M., and Gallagher, K.: Helium trapping in apatite damage: Insights from (U-Th-Sm)/He dating of different granitoid lithologies, Chem. Geol., 470, 116-131, https://doi.org/10.1016/j.chemgeo.2017.09.002, 2017.

Ritter, W., and Märk, T.D.: Optical studies of radiation damage and its annealing in natural fluorapatite, Nucl. Instr. Meth. Phys. Res. B1, 394-397, https://doi.org/10.1016/0168-583X(84)90098-3, 1984.

Shuster, D.L., Flowers, R.M., and Farley, K.A.: The influence of natural radiation damage on helium diffusion kinetics in apatite, Earth. Planet. Sci. Lett., 249, 148-161, https://doi.org/10.1016/j.epsl.2006.07.028, 2006.

Steiger, R.H., and Jäger, E.: Subcommission on geochronology: convention on the use of decay constants in geo- and cosmochronology, Earth Planet. Sci. Lett., 36, 359-362, https://doi.org/10.1016/0012-821X(77)90060-7, 1977.

Stockli, D.F., Linn, J.K., Walker, J.D., and Dumitru, T.A.: Miocene unroofing of the Canyon Range during extension along the Sevier Desert Detachment, west central Utah, Tectonics, 20, 289-307, https://doi.org/10.1029/2000TC001237, 2001.

Sturrock, C.P., Flowers, R.M., and Macdonald, F.A.: The Late Great Unconformity of the Central Canadian Shield, Geochem. Geophys. Geosys., 22, e2020GC009567, https://doi.org/10.1029/2020GC009567, 2021.

Tripathy-Lang, A., Hodges, K.V., Monteleone, B.D., and van Soest, M.C.: Laser (U-Th)/He thermochronology of detrital zircons as a tool for studying surface processes in modern catchments, J. Geophys. Res.: Earth Surf., 118, 1333-1341, https://doi.org/10.1002/jgrf.20091, 2013.

Troch, J., Ellis, B.S, Schmitt, A.K., Bouvier, A.-S., and Bachmann, O.: The dark side of zircon: textural, age, oxygen isotopics and trace element evidence of fluid saturation in the subvolcanic reservoir of the Island Park-Mount Jackson Rhyolite, Yellowstone (USA), Contrib. Min. Petrol., 173, 54, https://doi.org/10.1007/s00410-018-1481-2, 2018.

https://doi.org/10.5194/gchron-2024-1
Preprint. Discussion started: 25 January 2024

Vermeesch, P.: Three new ways to calculate average (U-Th)/He ages, Chem. Geol., 249, 339-347, https://doi.org/10.1016/j.chemgeo.2008.01.027, 2008.

Vermeesch, P.: HelioPlot, and the treatment of overdispersed (U-Th-Sm)/He data, Chem. Geol., 271, 108-111, https://doi.org/10.1016/j.chemgeo.2010.01.002, 2010.

Vermeesch, P.: Statistics for fission-track thermochronology, in: Fission-track thermochronology and its application to Geology, edited by: Malusà, M.G., and Fitzgerald, P.G., Springer International Publishing, New York, pp. 109-122, https://doi.org/10.1007/978-3-319-89421-8_6, 2019.

Vermeesch, P., and Tian, Y.: Thermal history modelling: HeFty vs. QTQt, Earth-Sci. Rev., 139, 279-290, https://doi.org/10.1016/j.earscirev.2014.09.010, 2014.

Vermeesch, P., Seward, D., Latkoczy, C., Wipf, M, Günther, D., and Bauer, H.: α-emitting mineral inclusions in apatite, their effect on (U-Th)/He ages, and how to reduce it, Geochim. Cosmochim. Acta, 71, 1737-1746, https://doi.org/10.1016/j.gca.2006.09.020, 2007.

Wendt, I., and Carl, C.: The statistical distribution of the mean squared weighted deviation, Chem. Geol., 86, 275-285, https://doi.org/10.1016/0168-9622(91)90010-T, 1991.

Wernicke, R.S., and Lippolt, H.J.: Botryoidal hematite from the Schwarzwald (Germany): heterogeneous uranium distributions and their bearing on the helium dating method, Earth Planet. Sci. Lett., 114, 287-300, https://doi.org/10.1016/0012-821X(93)90031-4, 1993.

Willett, C.D., Fox, M., and Shuster, D.L.: A helium-based model for the effects of radiation damage annealing on helium diffusion kinetics in apatite, Earth Planet. Sci. Lett., 477, 195-204, https://doi.org/10.1016/j.epsl.2017.07.047, 2017.

Wolfe, M.R., and Stockli, D.F.: Zircon (U-Th)/He thermochronometry in the KTB drill hole, Germany, and its implications for bulk He diffusion kinetics in zircon, Earth Planet. Sci. Lett., 295, 69-82, https://doi.org/10.1016/j.epsl.2010.03.025, 2010.

York, D.: Least squares fitting of a straight line with correlated errors, Earth Planet. Sci. Lett., 5, 320–324, https://doi.org/10.1016/S0012-821X(68)80059-7, 1968.

Zeigler, S.D., Metcalf, J.R., and Flowers, R.M.: A practical method for assigning uncertainty and improving the accuracy of alpha-ejection corrections and eU concentrations in apatite (U–Th) / He chronology, Geochronology, 5, 197-228, https://doi.org/10.5194/gchron-5-197-2023, 2023.